RESEARCH ARTICLE

ZapE Is a Novel Cell Division Protein Interacting with FtsZ and Modulating the Z-Ring Dynamics

Benoit S. Marteyn,[a,b] Gouzel Karimova,[c,d] Andrew K. Fenton,[e] Anastasia D. Gazi,[a,b] Nicholas West,* Lhousseine Touqui,[f] Marie-Christine Prevost,[g] Jean-Michel Betton,[h] Oemer Poyraz,[i] Daniel Ladant,[c,d] Kenn Gerdes,[e] Philippe J. Sansonetti,[a,b,j] Christoph M. Tang[k]

Institut Pasteur, Unité de Pathogénie microbienne Moléculaire, Paris, France[a]; Institut National de la Sante et de la recherche Medicale Unité 786, Paris, France[b]; Institut Pasteur, Unité de Biologie des Interactions Moléculaires, Paris, France[c]; CNRS UMR3528, Unité de Biologie des Interactions Moléculaires, Paris, France[d]; University of Newcastle, Centre for Bacterial Cell Biology, Newcastle-upon-Tyne, United Kingdom[e]; Institut Pasteur, Unité de Défense Innée et Inflammation, Paris, France[f]; Institut Pasteur, Imagopole/PFMU, Paris, France[g]; Institut Pasteur, Unité de Microbiologie Structurale, Paris, France[h]; Karolinska Institutet, Department of Medical Biochemistry & Biophysics, Stockholm, Sweden[i]; Collège de France, Paris, France[j]; University of Oxford, Sir William Dunn School of Pathology, Oxford, United Kingdom[k]

* Present address: Centenary Institute, Mycobacterial Research Laboratory, Newtown, NSW, Australia.

ABSTRACT **Bacterial cell division requires the formation of a mature divisome complex positioned at the midcell. The localization of the divisome complex is determined by the correct positioning, assembly, and constriction of the FtsZ ring (Z-ring). Z-ring constriction control remains poorly understood and (to some extent) controversial, probably due to the fact that this phenomenon is transient and controlled by numerous factors. Here, we characterize ZapE, a novel ATPase found in Gram-negative bacteria, which is required for growth under conditions of low oxygen, while loss of *zapE* results in temperature-dependent elongation of cell shape. We found that ZapE is recruited to the Z-ring during late stages of the cell division process and correlates with constriction of the Z-ring. Overexpression or inactivation of *zapE* leads to elongation of *Escherichia coli* and affects the dynamics of the Z-ring during division. *In vitro*, ZapE destabilizes FtsZ polymers in an ATP-dependent manner.**

IMPORTANCE **Bacterial cell division has mainly been characterized *in vitro*. In this report, we could identify ZapE as a novel cell division protein which is not essential *in vitro* but is required during an infectious process. The bacterial cell division process relies on the assembly, positioning, and constriction of FtsZ ring (the so-called Z-ring). Among nonessential cell division proteins recently identified, ZapE is the first in which detection at the Z-ring correlates with its constriction. We demonstrate that ZapE abundance has to be tightly regulated to allow cell division to occur; absence or overexpression of ZapE leads to bacterial filamentation. As *zapE* is not essential, we speculate that additional Z-ring destabilizing proteins transiently recruited during late cell division process might be identified in the future.**

Received 24 January 2014 **Accepted** 27 January 2014 **Published** 4 March 2014

Citation Marteyn BS, Karimova G, Fenton AK, Gazi AD, West N, Touqui L, Prevost M-C, Betton J-M, Poyraz O, Ladant D, Gerdes K, Sansonetti PJ, Tang CM. 2014. ZapE is a novel cell division protein interacting with FtsZ and modulating the Z-ring dynamics. mBio 5(2):e00022-14. doi:10.1128/mBio.00022-14.

Editor B. Brett Finlay, The University of British Columbia

Address correspondence to Philippe J. Sansonetti, psanson@pasteur.fr.

Cell division is a fundamental process that is central to cellular morphology and replication. Accurate division requires precise control of cell enlargement and of the timing and location of the site of division. The first protein found to localize at the midcell during division of prokaryotic cells was FtsZ, a GTPase that is structurally homologous to eukaryotic tubulin (1). FtsZ polymerizes at the midcell, forming a large ring-like network at the cell membrane known as the Z-ring (2). A mature divisome complex subsequently forms at the Z-ring and is composed of at least 10 proteins which are essential for cell division (3). These proteins include FtsZ, FtsA, FtsK, FtsQ, FtsL, FtsB, FtsW, FtsI, and FtsN. It is being increasingly appreciated that a number of accessory proteins are also recruited to the divisome and contribute to cell division and may be essential for growth, depending upon the specific environmental conditions. Several of these Z-ring-associated proteins (Zaps, i.e., ZapA, ZapB, ZapC, and ZapD [4–6]) modulate the dynamics of Z-ring assembly and stability. At present, little is known about cell division during growth under low-oxygen conditions, even though many bacteria thrive in anaerobic environments, particularly within mammalian hosts (7, 8).

Here we identify a further Z-ring-associated protein named ZapE which is required for cell division under low-oxygen conditions. ZapE is an ATPase present in Gram-negative bacteria that appears at the constricting Z-ring late in cell division. ZapE affects FtsZ multimerization and polymerization *in vitro*. *In vivo* ZapE recruitment correlates with Z-ring constriction.

RESULTS

Identification of ZapE, required for growth in the absence of oxygen. While screening a library of *Shigella flexneri* mutants for their ability to colonize the gastrointestinal (GI) tract (9, 10), we identified a mutant that was defective for colonization with a transposon 12 bp upstream of a 1,128-bp open reading frame (ORF) (accession number b3232; Fig. 1A). The role of this ORF

A

Strain	Description	C.I.
M90Tmut6	Transposon mutant *zapE*	< 0.01
M90T::Δ*zapE*	*zapE* mutant	0.03
M90T::Δ*zapE* + p*zapE*-GFP M90T	complemented mutant	0.31

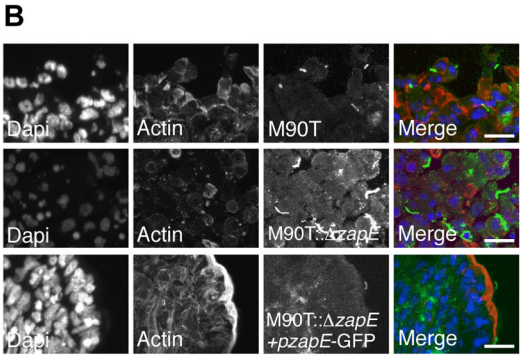

FIG 1 ZapE is required during the *Shigella* infectious process *in vivo*. (A) Competitive index (C.I.) of a *Shigella flexneri* 5A *zapE* transposon mutant (M90Tmut6), a *zapE* mutant (M90T::Δ*zapE*), and a complemented strain (M90T::Δ*zapE*/p*zapE*-GFP M90T) *in vivo*. The C.I. assessed the ability of each mutant to colonize the rabbit ileal loop in comparison with the wild-type strain. A C.I. of 1 indicates no attenuation. Data represent averages of the results of three independent experiments. (B) Immunodetection of the M90T, M90T::Δ*zapE*, and M90T::Δ*zapE*/p*zapE*-GFP strains in the rabbit ileal loop model. DNA was stained with DAPI (blue) and actin with RRX-phalloidin (red). *Shigella* strains were labeled using α-LPS polyclonal antibody (pAb) (green). Image acquisition was performed using a confocal microscope. Right-hand panels show enlarged areas. Bars are 5 μm.

(here designated ZapE) in colonization was confirmed by construction and analysis of a deletion mutant (M90T::Δ*zapE*) and by complementation (Fig. 1; see also Fig. S1A and Tables S1A and B in the supplemental material). Of note, examination of tissues from infected animals demonstrated that *S. flexneri* M90T::Δ*zapE* displayed an elongated cellular phenotype in the GI tract (Fig. 1B).

To further characterize the contribution of ZapE to cell division, we examined the phenotype of an *Escherichia coli* MG1655 mutant (K12::Δ*zapE*) grown under a variety of conditions relevant to survival of bacteria *in vivo*. Strikingly, while *E. coli* lacking ZapE had no demonstrable growth defect in aerobic conditions, the mutant was defective for growth in anaerobiosis (Fig. 2A; see also Fig. S1B and C in the supplemental material); complementation analysis confirmed that loss of ZapE was responsible for the failure to grow in a low-oxygen environment. Additionally, growth at elevated temperatures (i.e., 42°C) led to an exaggerated elongation of *E. coli* lacking ZapE (Fig. 2B). The temperature-dependent elongated phenotype was also observed in *Shigella*—with or without a virulence plasmid (INV−)—as well as in *E. coli*, comparing growth at 30°C and 42°C (Student's *t* test; $P < 0.001$) (see Fig. S2A and B). The K12::Δ*zapE* phenotype was confirmed using a K12::Δ*zapE*::Km-p*zapE* strain in the presence of glucose but not of arabinose, allowing functional complementation of the phenotype (see Fig. S3A).

ZapE is an ATPase that interacts with components of the divisome. ZapE is found in Gram-negative bacteria (see Table S1C in the supplemental material) and is predicted to contain putative Walker A (GGVGRGK$_{84}$T) and Walker B nucleotide-binding sites (see Fig. S3B in the supplemental material). Therefore, we examined the capacity of ZapE to hydrolyze ATP and GTP. We found that purified recombinant ZapE hydrolyzed ATP but not GTP (Fig. 2C). Introduction of a single amino acid substitution in the ATP-binding site (in ZapE$_{K84A}$) abolished ATPase activity (Fig. 2C). In addition, we modeled the organization of the active site of ZapE by small-angle X-ray scattering (SAXS) analysis (Fig. 2D; seen also Fig. S3C to E), using fold recognition methods based on the extended AAA+ ATPase domain of the ATP-dependent metalloprotease FtsH (PDB identification number [ID] 2CE7). As FtsZ is a known FtsH substrate (11, 12), the structural similarity between ZapE and FtsH suggests that ZapE might interact directly with FtsZ.

To further define the role of ZapE during cell division, we examined whether the protein interacts with components of the divisome, including FtsZ. Using a bacterial two-hybrid (BACTH) system (13), we identified potential interactions between ZapE and FtsQ, FtsL, FtsI, and FtsN (Fig. 3A) ($P < 0.01$ and $P < 0.001$, Student's *t* test). In contrast, no interaction was observed with FtsA, which forms actin-like protofilaments (14), and FtsK, which coordinates DNA segregation with division (15). A similar result was obtained using ZapE from *S. flexneri* (M90T) as bait paired with these *E. coli* division proteins (Fig. 3A). Interactions of ZapE with FtsZ could not be examined by the BACTH system, as expression of both T18-*zapE* or T25-*zapE* and T18-*ftsZ* together was toxic (not shown and reference 16).

To confirm interactions identified by BACTH analysis, pulldown assays were performed with *E. coli* His-tagged ZapE bound to beads and green fluorescent protein-FtsQ (GFP-FtsQ), GFP-FtsL, GFP-FtsI, and GFP-FtsN expressed in *E. coli* (Fig. 3B); no interaction was observed when GFP was expressed on its own. In addition, pulldown assays with bound ZapE or ZapE$_{K84A}$ isolated FtsZ-GFP from cell lysates (Fig. 3B), indicating that the ZapE ATP binding site was not required for FtsZ interaction *in vitro*.

ZapE was found in the cytoplasm, and further localization by electron microscopy (EM) analysis revealed that most of the signal was detected in the vicinity of the bacterial inner membrane (see Fig. S4A in the supplemental material) ($P < 0.001$, Student's *t* test); this observation is consistent with an interaction with FtsZ.

ZapE localizes to the constricting Z-ring toward the end of cell division. Next, we performed time-lapse microscopy to determine the temporal and spatial association of ZapE in relation to FtsZ at the single-cell level. To achieve this, ZapE-mCherry was expressed under the control of its native promoter (see Fig. S4B in the supplemental material) in a *zapE* mutant containing FtsZ-GFP (carried on pDSW230) (17). Of note, ZapE was detected only at the Z-ring and exclusively during the later stages of cell division (Fig. 3C; see also Movie S1 in the supplemental material). Indeed, the appearance of ZapE at the midcell coincided with constriction of the Z-ring and with its subsequent disappearance (see Fig. S4C). In events leading up to the maximalization of Z-ring constriction (defined as t_0), FtsZ levels increased in a stepwise fashion as the diameter of the Z-ring diminished; the amount of ZapE present at the Z-ring increased progressively until maximal constriction of

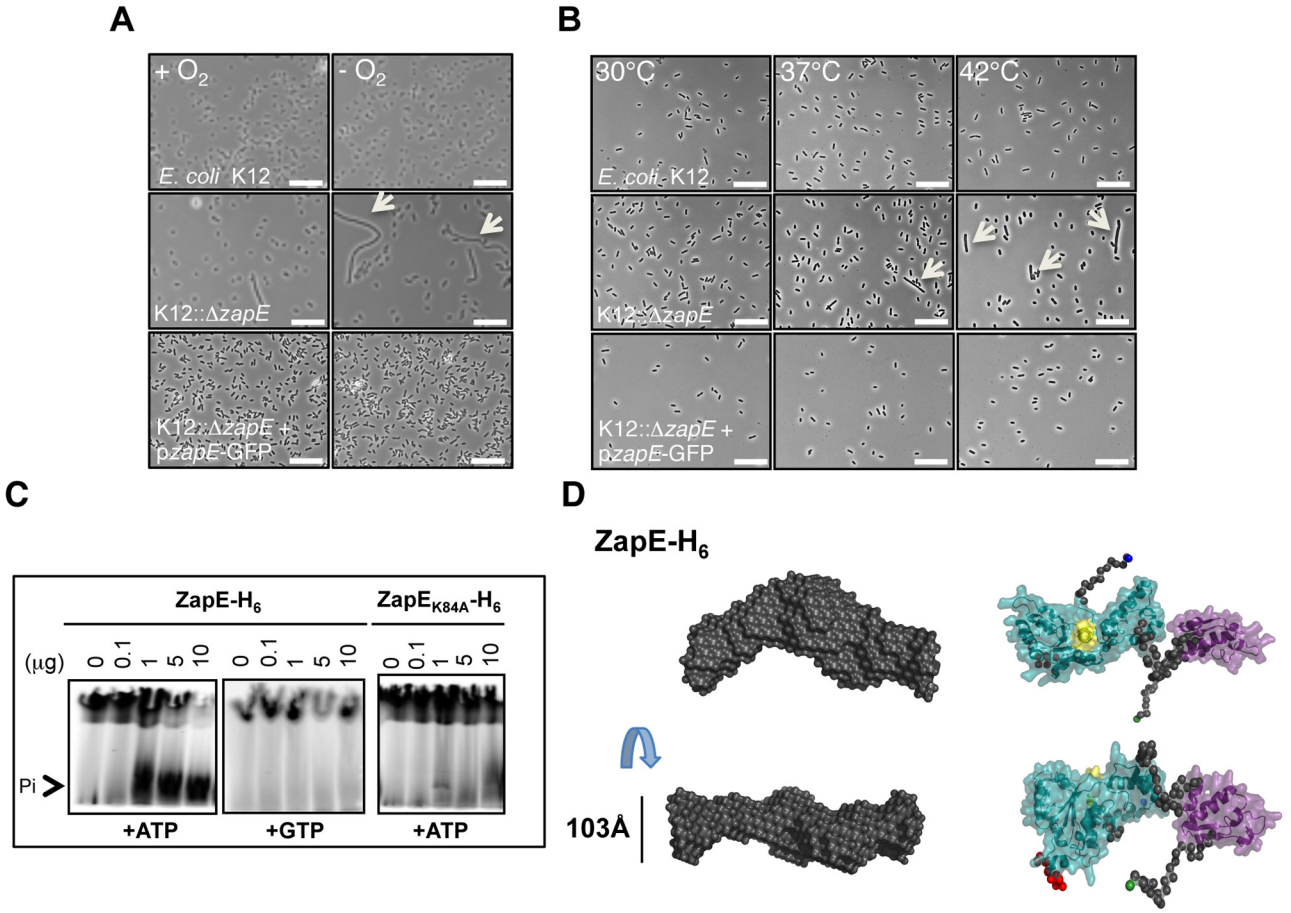

FIG 2 *zapE* inactivation leads to a stress-dependent (anaerobiosis, temperature) elongated phenotype of *E. coli*. *zapE* encodes an ATPase. (A) Anaerobiosis-dependent phenotype of *E. coli* wild-type, Δ*zapE* mutant, and complemented strains. Growth of K-12, K12::Δ*zapE*, and K12::Δ*zapE*/p*zapE*-GFP strains in minimum media in the presence ($+O_2$) or absence ($-O_2$) of oxygen at 37°C is shown. Scale bars are 10 μm. Arrows indicate elongated bacteria. (B) Temperature-dependent phenotype of K-12, K12::Δ*zapE*, and K12::Δ*zapE*/p*zapE*-GFP strains. Bacteria were grown in rich media at the indicated temperature until an $OD_{600} = 0.5$ was reached. Scale bars are 10 μm. Arrows indicate elongated bacteria. **, $P < 0.01$; *, $P < 0.05$. (C) ZapE or $ZapE_{K84A}$ ATPase activity assessed by silica layer chromatography. The reaction was performed in a Tris-HCl buffer (50 mM; pH 7.4) containing 10 mCi of radiolabeled ATPγ32 (or GTPγ32), 10 mM ATP, and 2.5 mM $MgCl_2$ in the presence of various ZapE-H_6 or $ZapE_{K84A}$-H_6 quantities, as indicated. (D) Most probable atom model of 15 DAMMIN reconstructions fitting the data at up to $s_{max} = 0.24$ Å $^{-1}$ with an $x = 1.683$ and an NSD value of 0.7 ± 0.024, indicating the stability of the solution. The Walker A motif in the AAA+ ATPase is highlighted in yellow. N-terminal and C-terminal residues of ZapE are highlighted in green and blue.

the Z-ring occurred (Fig. 3D) (Student's *t* test; $P < 0.001$), demonstrating a clear correlation between the expression and localization of ZapE and Z-ring constriction *in vivo*.

ZapE abundance modulates Z-ring stability. We next examined whether modulating levels of ZapE within cells affected their shape and the appearance of Z-rings. Initially, the location of FtsZ-GFP during cell division was examined in either the presence or the absence of ZapE. FtsZ-GFP does not fully complement an *ftsZ* mutant, but localizes to the midcell, and does not impair normal cell division when expressed at basal levels in wild-type bacteria (18). Loss of ZapE in a strain expressing FtsZ-GFP led to marked filamentation, with the loss of ordered Z-rings in cells (Fig. 4A [rich media] and B [minimum media]; see also Fig. S5A and Movie S2 in the supplemental material [live microscopy]). This filamentation was more pronounced during growth at higher temperatures (Fig. 4A) and during the stationary phase (Fig. 4C). We confirmed that filamentation in cells lacking ZapE was more marked following overexpression of native FtsZ in a dose-dependent manner (Fig. 4D).

Loss of ZapE in a strain expressing FtsZ-mCherry led to the formation of multiple disorganized FtsZ rings found sporadically along the length of the extended bacteria compared to the wild-type strain (Fig. 5A). Furthermore, we examined the effect of overexpressing ZapE under the control of an IPTG (isopropyl-β-D-thiogalactopyranoside)-inducible promoter. In wild-type cells, ZapE overexpression also resulted in dose-dependent filamentation (Fig. 5B and C; see also Fig. S5B in the supplemental material). However, no Z-rings (detected with FtsZ-mCherry) were detected along the length of filaments when ZapE overexpression was induced with high levels of IPTG (Fig. 5A; see also Fig. S5C [as a control, without IPTG]), although additional adverse effects of ZapE overexpression could not be ruled out. This was not observed in cells overexpressing $ZapE_{K84A}$, which exhibited normal bacterial shape and single ordered Z-rings (Fig. 5A). Taken together, these data are consistent with ZapE and FtsZ having antagonizing roles at the Z-ring inside cells.

ZapE impairs the stability of polymerized FtsZ *in vitro*. Next we examined the effect of ZapE on polymerized FtsZ *in vitro* using

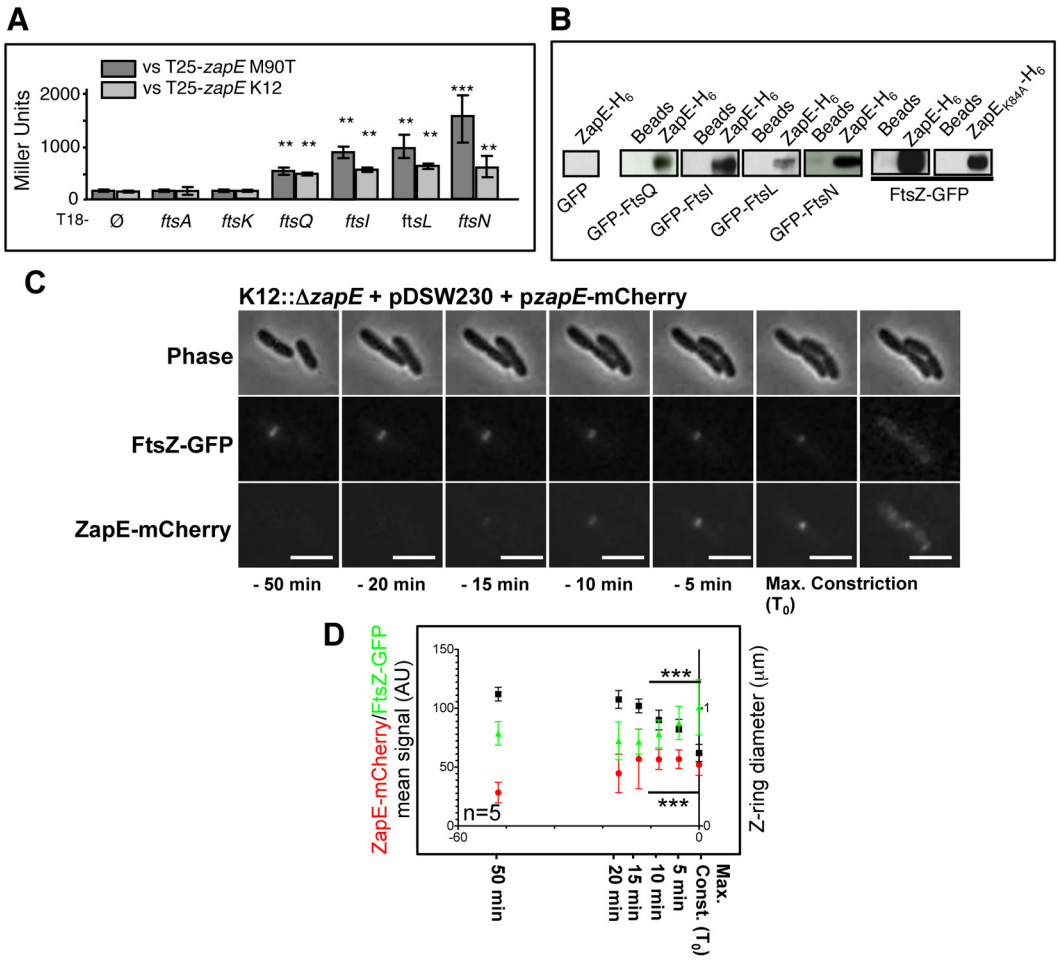

FIG 3 ZapE is a cytoplasmic protein which interacts with FtsZ *in vitro* and *in vivo*. ZapE recruitment correlates with Z-ring constriction. (A) BACTH analysis was performed using the T25-*zapE* K-12 (*E. coli* K-12) or T25-*zapE* M90T (*Shigella* M90T) versus T18-plasmid constructs with indicated genes. Results are expressed in Miller units and were averaged from three independent experiments. Error bars show the standard deviations (SD). Comparing average activity to that of the T18 negative control, ** indicates $P < 0.01$ and *** indicates $P < 0.001$ (Student's *t* test). (B) Pulldown assay with K-12 ZapE-H_6 and GFP or GFP-tagged proteins in *E. coli* lysates. The interaction between *E. coli* FtsZ-GFP (pDSW230) and *E. coli* ZapE-H_6 and $ZapE_{K84A}$-H_6, respectively, was analyzed using a His pulldown assay. (C) Expression and localization of FtsZ-GFP and ZapE-mCherry during a cell division. Time-lapse observation was performed on an LB-agar pad at 30°C, using a 200 M Axiovert epifluorescence microscope (Zeiss). Image acquisition was performed every 3 min (see also Movie S1 and Fig. S4C in the supplemental material for raw fluorescence quantification). This result is representative of five individual observations from three independent experiments. Bars are 2 μm. Max, maximum. (D) Relationship between, respectively, ZapE-mCherry and the FtsZ-GFP mean signal (AU) (K12::Δ*zapE* p*zapE*-mCherry) and the Z-ring diameter (pDSW230). Mean FtsZ-GFP and ZapE-mCherry fluorescent signals are represented in Fig. S4C in the supplemental material. $n = 5$ independent observations; error bars show the SD. *** indicates $P < 0.001$ (Student's *t* test). Max. Const., maximum constriction.

purified recombinant proteins. As described previously (19), in the presence of GTP and Ca^{2+} purified FtsZ and FtsZ-GFP form small polymers *in vitro* (Fig. 5D; see also Fig. S5D in the supplemental material). The addition of ZapE promoted the polymerization of FtsZ/FtsZ-GFP through large helical structures (Fig. 5D; see also Movie S3). These structures were no longer stable when ATP was added with ZapE after a 3-min incubation (Fig. 5D), while $ZapE_{K84A}$ had no effect (Fig. 5D), indicating that active ZapE reduces the stability of FtsZ polymers in the presence of ATP through a molecular mechanism which remains to be defined.

DISCUSSION

Here, we identified and characterized a novel Z-ring-associated protein named ZapE, which is an ATPase found among Gram-negative bacteria (see Table S1C in the supplemental material). ZapE is not essential in *E. coli* or in *Shigella* during growth under standard laboratory conditions. However, in the absence of oxygen or at temperatures over 37°C, the contribution of ZapE to cell division becomes evident, with cells lacking this protein displaying a growth defect and elongated phenotype (Fig. 2A and B). The latter was detected in tissue sections of the GI tract infected with a *Shigella zapE* mutant; as a likely consequence of the cell division defect, *zapE* is required for efficient colonization of GI track (Fig. 1A and B). Therefore, the identification of ZapE from studies of bacteria *in vivo* indicates that examining bacteria in the environments that they encounter outside the laboratory could uncover the function of other accessory cell division proteins. In the future, studies of bacterial cell division under other growth conditions such as low pH, oxidative stress, or amino acid starvation will reveal novel aspects of cell division regulation allowing bacterial survival during host invasion.

Several ATPases targeting FtsZ during cell division such as

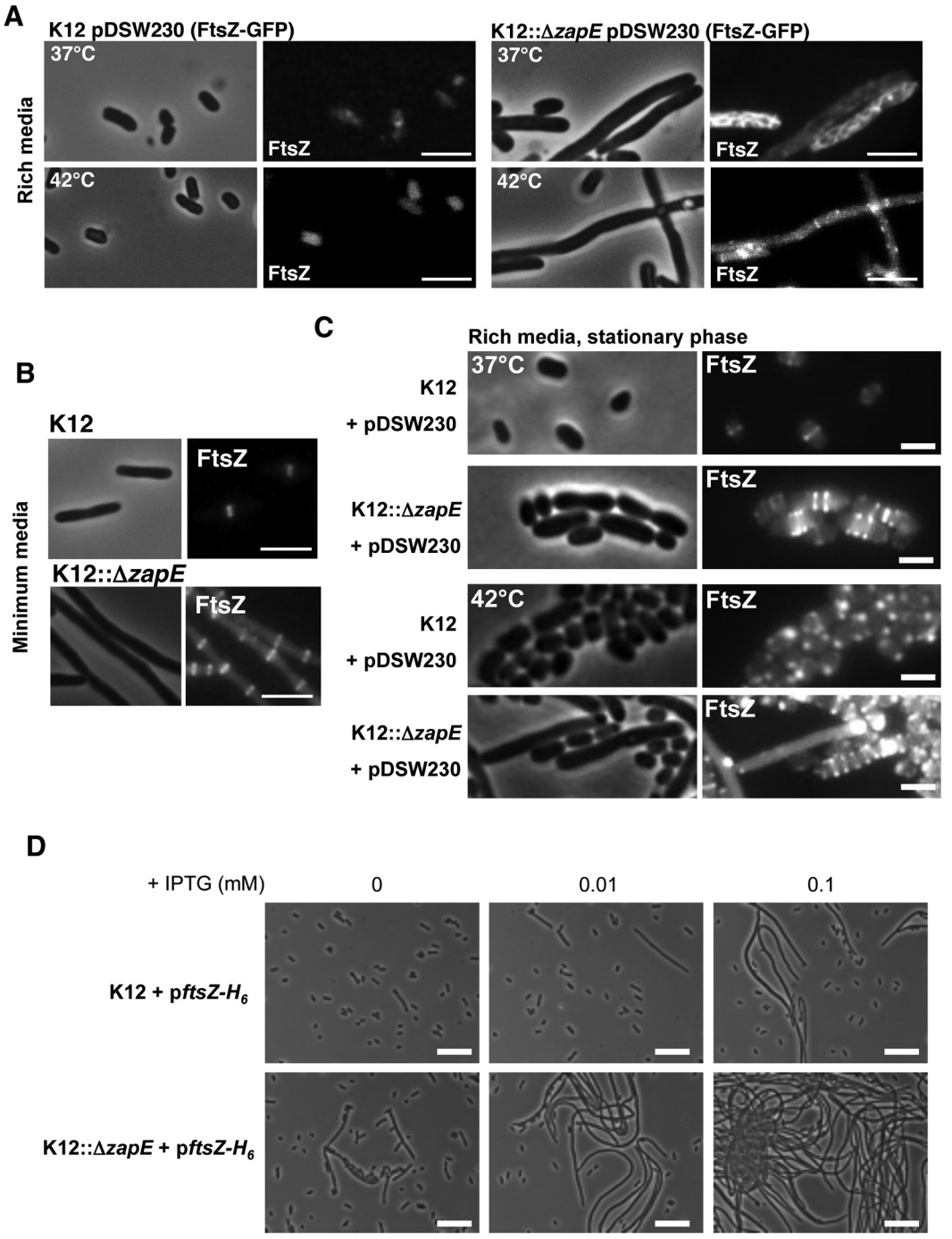

FIG 4 Effect of ZapE inactivation on K-12 shape upon FtsZ-GFP and FtsZ expression modulation. (A) Localization of FtsZ-GFP (pDSW230) in K-12 and K12::Δ*zapE* strains grown in rich media (LB) at 37°C or 42°C in the absence of IPTG until an OD_{600} = 0.5 was reached. Bars are 5 μm. (B) Localization of FtsZ-GFP (pDSW230) in K-12 and K12::Δ*zapE* strains grown in minimum media (M9) at 37°C in the absence of IPTG until an OD_{600} = 0.5 was reached. Bars are 2 μm. (C) FtsZ-GFP (pDSW230) localization in K-12 and K12::Δ*zapE* strains during the stationary phase performed in LB rich media at 37°C or 42°C. These observations are representative of the results of at least three independent experiments. Bars are 1 μm. (D) Effect of FtsZ-H_6 (WM971) overexpression on K-12 and K12::Δ*zapE* shape. Bacteria were grown in LB at 37°C in the presence of the indicated concentrations of IPTG until an OD_{600} = 0.5 was reached. These observations are representative of the results of three independent experiments. Bars are 10 μm.

FtsH, MinD, and KaiC are involved in cell division functions. FtsH is an ATP-dependent zinc metalloprotease targeting FtsZ *in vitro* (11), although this activity could not be confirmed *in vivo* (12). MinD belongs to the Min system involved in Z-ring positioning (20). KaiC inhibits Z-ring formation controlling the circadian clock in *Synechococcus elongatus* (21). None of these ATPases have proven functions in the dynamics of Z-ring constriction *in vivo*. Indeed, if starting events of cell division (Z-ring assembly and

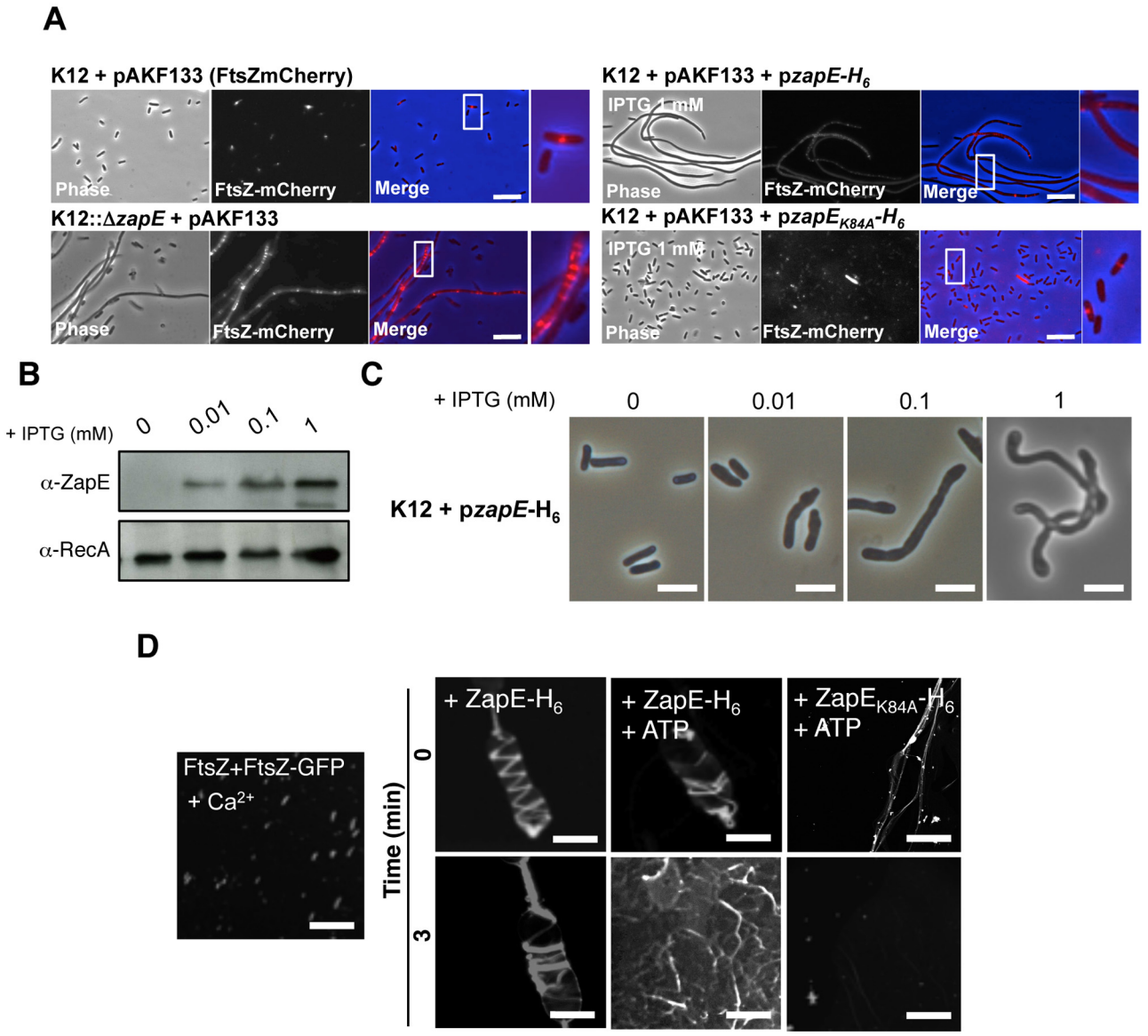

FIG 5 ZapE level of expression perturbates Z-ring stability and bacterial shape. (A) Effect of *zapE* inactivation and ZapE or $ZapE_{K84A}$ overexpression on Z-ring stability (FtsZ-mCherry, pAKF133). Bacteria were grown in minimum media at 37°C in the presence of arabinose (0.01%) in addition to IPTG (1 mM) when indicated. Data are representative of the results of four independent observations (see also Fig. S5C in the supplemental material). (B) ZapE-H_6 level of expression in strain K12-p*zapE*-H_6 grown in LB at 37°C in the presence of the indicated concentrations of IPTG until an $OD_{600} = 0.5$ was reached. The level of expression of ZapE-H_6 was assessed by Western blot analysis on bacterial whole extract using a polyclonal α-ZapE antibody. α-RecA was used as a control. (C) Phenotypic characterization of strain K12-p*zapE*-H_6 grown under the conditions described for panel B. These observations are representative of the results of three independent experiments. Bars are 2 μm. (D) Polymerization of FtsZ (10 μM) with FtsZ-GFP (5 μM) *in vitro* was performed over 3 min, in the presence of 10 mM $CaCl_2$, as described in references 16 and 19. ZapE-H_6 or $ZapE_{K84A}$-H_6 (10 μM) was subsequently added to the reaction mixture ($t = 0$), with ATP added when indicated. Confocal imaging was performed at 0 and 3 min. Data are representative of the results of three independent experiments. Bars are 5 μm.

positioning) have been well characterized (22), events leading to the disappearance of the ring and completion of division have not been defined in as much detail and remain to be discussed (23). This might be explained by the transiency of the Z-ring constriction phenomenon. Consistently, ZapE fusion (mCherry) recruitment at the Z-ring could be seen in this study only by live microscopy (Fig. 3C; see also Movie S1 in the supplemental material).

We observed that in the presence of ATP and Ca^{2+}, ZapE promoted bundling of FtsZ/FtsZ-GFP polymers into unstable three-dimensional structures (Fig. 5D; see also Movie S3 in the supplemental material). A structural homology between ZapE and FtsH was found by SAXS analysis (Fig. 2D). This observation should support further investigations on how ZapE directly or indirectly affects the effect of activity on Z-ring constriction, accounting for the destabilization observed *in vitro* (Fig. 5D) and *in vivo* upon ZapE overexpression (Fig. 4A).

The precise control of the ZapE level appears to be crucial for Z-ring stability and dynamics as we showed that either ZapE loss or overexpression (Fig. 4A) altered Z-ring stability and led to bacterial filamentation. Further studies should aim at defining ZapE

abundance regulation (expression and degradation) during the cell division process and its consequences for Z-ring stability to better characterize the role of ZapE in the Z-ring dynamic *in vivo*.

MATERIALS AND METHODS

Bacterial strains and growth conditions. The bacterial strains and plasmids used in this study are described in Table S1A in the supplemental material. *Shigella* strains were grown in Trypticase soy (TCS) broth or on TCS agar plates supplemented with 0.01% Congo red (Sigma). *E. coli* strains were grown in LB media. Anaerobic growth experiments were performed in a Mini Macs MG-250 chamber (Don Withley). D-Glucose and L-arabinose were used at a concentration of 0.2% to modulate the expression of genes cloned under the control of the pBAD33 promoter.

Expression plasmid construction. The pSUC vector construction was achieved by amplifying the mCherry fusion from the pmCherry-N1 vector using the SG150 and SG151 primer pair (see Table S1B in the supplemental material), introducing the BamHI and EcoRI restriction sites. The pSU19 vector was digested with BamHI and EcoRI restriction enzymes prior ligation of the digested mCherry amplified fragment, leading to the generation of the pSUC vector (see Fig. S4B). This expression vector allows the expression of mCherry protein fusions in the C terminus under the control of the promoter of the gene of interest in *E. coli* and in *Shigella*.

Expression of the FtsZ-GFP fusion under the control of a *lac* promoter was performed using either the pDSW230 and pDSW231 construct (kindly provided by David Weiss) (described in Table S1A in the supplemental material). FtsZ-mCherry fusion expression under the control of an arabinose-inducible promoter was performed with pAKF133 (described in Table S1A).

DNA manipulations. The initial transposon insertion in *S. flexneri* M90T in *zapE* was performed as described previously (9). The construction of inactivated *zapE* mutants was then performed in *E. coli* and *S. flexneri*.

Δ*zapE* mutant construction. In MG1655, *E. coli* K-12 P1vir page lysate was prepared on the JW3201 donor strain from the Keio collection (1, 24). In the JW3201 strain, the *zapE* ORF is substituted by the kanamycin (Km) resistance marker (Δ*zapE*::Km) (2, 24). The Δ*zapE*::Km cassette was introduced into MG1655 by P1 transduction (3, 25), and selection for kanamycin-resistant (Km^r) colonies was made on LB plates containing kanamycin (50 μg/ml). After reisolation, several clones were verified by PCR to confirm the right chromosomal structure of the Δ*zapE*::Km deletion. One clone was chosen and named K12Δ*zapE*::Km.

K12::Δ*zapE* was then obtained from K12Δ*zapE*::Km by removing the kanamycin resistance marker from the Δ*zapE*::Km cassette. In this Δ*zapE*::Km cassette, the antibiotic resistance marker is flanked by two direct *frt* repeats, which are the recognition targets for the site-specific recombinase FLP (4, 24). Therefore, to get rid of the resistance marker from the K12::Δ*zapE*::Km chromosome, pCP20, a temperature-sensitive plasmid that encodes the FLP recombinase, was used (5, 26). Briefly, K12Δ*op1*::Km cells were transformed with pCP20, and chloramphenicol-resistant (Cm^r) colonies were selected at 30°C on LB plates containing the corresponding antibiotic (30 μg/ml). Several of these clones were grown overnight on antibiotic-free LB plates at 42°C. Ten independent colonies were selected, and after single-colony passage at 30°C, all 10 colonies were no longer Cm^r and Km^r, indicating simultaneous loss of pCP20 and the kanamycin resistance marker from the bacterial chromosome. This FLP-catalyzed excision created an in-frame deletion of the *zapE* ORF, leaving behind a 102-bp scar sequence (Δ*zapE*::*frt*) (6, 24). To confirm the correct chromosomal structure of the Δ*zapE*::*frt* deletion, several Cm^s and Km^s clones were tested by PCR using the NWpr40 and NWpr41 primer pair (see Table S1B in the supplemental material). After confirmation, one clone was chosen and named K12::Δ*zapE*.

Alternatively, the Δ*zapE*::Km cassette was introduced into MG1655 expressing p*zapE* (pBAD33-*zapE*) by P1 transduction (7, 25), and selection for kanamycin-resistant (Km^r) colonies was performed on LB plates containing kanamycin (50 μg/ml). The K12::Δ*zapE*::Km p*zapE* strain was obtained.

In order to inactivate *zapE* in *Shigella flexneri* (M90T), a one-step chromosomal inactivation method was used to target homologous region for integration. Therefore, we generated PCR products with much longer flanking sequence using the K12::Δ*zapE* null mutant as the template. The M90T was transformed with PCR products amplified from K12::Δ*zapE*::Km mutant genomic DNA using primers NWpr23 and NWpr24 (see Table S1B in the supplemental material). The NWpr23 and NWpr24 primers were designed to include 50 bp of upstream and downstream sequence flanking *zapE*. This product was transformed into M90T::pKD46, which resulted in all kanamycin-resistant colonies containing the 1.50-kb kanamycin resistance gene as analyzed by PCR. Thus, an *S. flexneri* null mutant (M90T::Δ*zapE*) was successfully generated.

Expressing, respectively, a *zapE-GFP* and a *zapE-mCherry* fusion under the control of the *zapE* promoter resulted in the complementation of the M90T::Δ*zapE* and K12::Δ*zapE* mutants. In order to express a ZapE-GFP fusion, the *zapE* genes of *Shigella* and *E. coli* and their promoters (~500 bp) were amplified with the SG127 and SG128 primer pair (see Table S1B in the supplemental material) and cloned into pFpV25 vector digested with the BamHI and NdeI restriction enzymes. The p*zapE*-GFP M90T and p*zapE*-GFP K-12 constructs were obtained and sequenced (Table S1A).

In order to express *zapE-mCherry*, the *zapE* gene and its promoter (~500 bp) were amplified with the SG219 and SG155 primer pair (see Table S1B in the supplemental material) and cloned in pSUC vector digested with the HindIII and XbaI restriction enzymes (see Fig. S4B). The K84A point mutation of *zapE* was performed using the SG114 and SG115 primer pair (see Table S1B). p*zapE*-mCherry and p$zapE_{K84A}$-mCherry constructs were obtained and sequenced (see Table S1A).

In order to overproduce the ZapE-H_6 and $ZapE_{K84A}$-H_6 protein fusions in an IPTG-dependent manner, the corresponding *zapE* DNA fragments were amplified by PCR prior cloning in the pKJ1 plasmid digested using the NcoI and BamHI restriction enzymes (see Table S1A in the supplemental material). *zapE* was amplified using the SG90 and SG91 primer pair (see Table S1B), and $zapE_{K84A}$ was obtained using the SG114 and 1G115 primer pair to introduce a K84A single point mutation (see Table S1B). The resulting p*zapE*-H_6 and p$zapE_{K84A}$-H_6 constructs were analyzed by PCR and sequenced.

Rabbit ligated ileal loop model. New Zealand White rabbits weighting 2.5 to 3 kg (Charles River Breeding Laboratories, Wilmington, MA) were used for experimental infections. For each animal, up to 12 intestinal ligated loops, each 5 cm in length, were prepared as described previously (8, 9, 27). For the evaluation of the competitive index (C.I.), equal quantities of the wild-type strain and of the mutant were injected in each loop (corresponding to a total dose of 10^5 CFU per loop). After 16 h, animals were sacrificed and the luminal fluid was aspirated and *S. flexneri* recovered. The C.I. was calculated as the proportion of mutant to wild-type bacteria recovered from animals divided by the proportion of mutant to wild-type bacteria in the inoculums, and results are expressed as the means of the results determined with at least 4 loops from two independent animals. The experimental protocol was approved by the French Ethic Committee Paris 1 (number 20070004, 9 December 2007).

For immunohistochemical staining, infected rabbit ileum samples were washed in phosphate-buffered saline (PBS), incubated at 4°C in PBS containing 12% sucrose for 90 min and then in PBS–18% sucrose overnight, and frozen in optimum cutting temperature (O.C.T.) compound (Sakura) on dry ice. Sections (7 μm in thickness) were obtained using a CM-3050 cryostat (Leica). Fluorescent staining was performed using a rabbit anti-*Shigella* lipopolysaccharide (LPS) primary antibody (P. Sansonetti, Institut Pasteur) (1:200 dilution) and an anti-rabbit fluorescein isothiocyanate (FITC)-conjugated secondary antibody (1:1,000). Epithelium cell nuclei were stained with DAPI (4[prime],6-diamidino-2-

phenylindole) (1:1,000) and actin stained with Rhodamine Red-X (RRX)–phalloidin (1:1,000). Image acquisition was performed using laser scanning confocal microscopy. Image analysis was performed using ImageJ software.

Two-hybrid screen. We used the BACTH system that is based on the interaction-mediated reconstitution of an adenylate cyclase (AC) enzyme in the otherwise defective DHM1 *E. coli* strain (9, 13, 28). This system is composed of two replication-compatible plasmids, pKT25 and pUT18, respectively encoding the intrinsically inactive N-terminal T25 domain and C-terminal T18 domain of the AC enzyme. *E. coli* and *Shigella zapE* was amplified using the NG1281 and NG1282 primer pair and cloned in pKT25 vector.

pKT25 and pUT18 plasmids were subsequently doubly transformed to DHM1 to search for the AC reconstitution that turns on β-galactosidase production, leading to the production of blue color after 2 days of growth at 30°C on indicator plates containing X-Gal (5-bromo-4-chloro-3-indolyl-β-D-galactopyranoside) (Eurobio) (40 mg ml-1), isopropyl-1-thio-β-D-galactopyranoside (Invitrogen) (0.5 mM), Ap, Km, and nalidixic acid. β-Galactosidase activity was measured as described before, averaged from three independent experiments, and expressed as Miller units (10, 13, 29).

Antibody—α-ZapE antibody production. An α-ZapE rabbit polyclonal antibody was collected from two New Zealand White rabbits challenged with purified ZapE-H_6 (2 mg/ml solution) on four occasions separated by 2 weeks rest. The first injection (intradermal; 500 μl) was performed with the purified protein (125 μg) and with complete Freund's adjuvant. The second injection was performed following a similar procedure in the presence of incomplete Freund's adjuvant. The third and the last injections were performed with no adjuvant. The final blood collection was performed by cardiac puncture using a heparin-free tube. Sera were separated from blood cells by centrifugation (14,000 rpm, 30 min). α-FtsZ rabbit polyclonal antibody was kindly provided by Kenn Gerdes (4, 13, 17).

TLC analysis. ATPase and GTPase assays were performed in the presence of bovine serum albumin (BSA) (Sigma) (1.25 mg/ml), ATPγ32 or GTPγ32 (PerkinElmer) (30 μCi), ATP or GTP (Sigma) (50 mM), and 0.1 to 10 μg of purified ZapE-H_6 and $ZapE_{K84A}$-H_6 as indicated. The final reaction mixture volume was 20 μl in TMD buffer (25 mM Tris [pH 7.4], 10 mM $MgCl_2$, 1 mM dithiothreitol [DTT]). The reaction was run during 10 min at 37°C and stopped by the addition of 20 μl methanol. When indicated, chromatography was performed on thin-layer chromatography (TLC) plates (Thomas Scientific), with a mobile phase containing a mixture of lithium chloride (LiCl) and formic acid. After migration, a film was exposed on the plate and further developed. Radiolabeled Pi presence through ATPγ32 hydrolysis was then revealed.

Protein expression and purification. ZapE-H_6 and $ZapE_{K84A}$-H_6 protein fusions were expressed using the p*zapE*-H_6 K-12 and p$zapE_{K84A}$-H_6 K-12 constructs (see Table S1A in the supplemental material) expressed in an *E. coli* BL21(DE3) strain. Overnight cultures were subcultured in fresh LB media (1:100) and grown at 37°C until an optical density at 600 nm (OD_{600}) of 0.5 was reached. Overexpression was induced by the addition of 0.5 mM IPTG and was performed overnight at room temperature (RT). His-tagged proteins were purified on Talon beads (Clontech) and further purified by gel filtration using a Hiload 16/60 Superdex 200 column (GE) and a Tris buffer (50 mM; pH 7.5) containing 5 mM $MgCl_2$, 1 mM EDTA, and 0.1 M NaCl. FtsZ and FtsZ-GFP were purified by ion exchange on a Hiload 16/10 DEAE column using a Tris buffer (50 mM; pH 7.5) containing 5 mM $MgCl_2$, 1 mM EDTA, and 0.1 M NaCl (buffer 1) and a Tris buffer (50 mM; pH 7.5) containing 5 mM $MgCl_2$, 1 mM EDTA, and 1 M KCl (buffer 2) as described previously (14, 30), followed by a gel filtration, as described above.

His pulldown assay. ZapE-H_6 or $ZapE_{K84A}$-H_6 fusions (30 μg) were incubated on Talon beads for 1 h at 4°C in resuspension buffer (20 mM Tris-HCl [pH 8], 100 mM NaCl), supplemented with a protease inhibitor cocktail (Roche). Unbound proteins were removed by washing twice using the resuspension buffer. Extracts containing GFP fusions (FtsZ, FtsQ, FtsL, FtsI, and FtsN) were prepared from bacterial cultures grown in LB at 37°C in the presence of 1 mM IPTG for 3 h. Bacterial pellets were resuspended in a Tris-HCl buffer (50 mM) supplemented with a protease inhibitor cocktail (Roche) and sonicated. The resulting suspensions were centrifuged at 12,000 × *g* for 30 min, and supernatants were collected. In each pulldown experiment, 10 μg of *E. coli* soluble extract containing GFP fusions (FtsZ, FtsQ, FtsL, FtsI, and FtsN) was incubated during 1 h at 4°C. After 3 washes with resuspension buffer, 2× sample buffer was added and the beads were boiled and subjected to SDS-PAGE gel analysis. As controls, extracts were incubated with Talon beads only.

FtsZ/FtsZ-GFP polymerization *in vitro*. Fluorescent FtsZ/FtsZ-GFP polymers were generated in a buffer containing 50 mM HEPES, 50 mM KCl, 5 mM $MgCl_2$, and 10 mM $CaCl_2$ in addition to 1 mM GTP. Polymerization of FtsZ (10 μM) and FtsZ-GFP (5 μM) occurred during 0 to 3 min at 30°C on glass slides. Then, ZapE-H_6 or $ZapE_{K84A}$-H_6 (10 μM) and ATP (1 mM) were added when indicated to reach a final volume of 100 μl. Polymer imaging was performed using a TCS SP5 confocal microscope (Leica).

Western blot analysis. Bacterial extracts were prepared as follows. For FtsZ, ZapE, and RecA detection in K-12 and K12::Δ*zapE* strains, overnight bacterial cultures were subcultured in 100 ml LB liquid media at 37°C until the OD at A_{600} reached 0.3. Bacteria were harvested by centrifugation for 15 min at 3,000 × *g*, washed, and then resuspended in 10 ml PBS. Cells were spun again for 5 min at 3,000 × *g* and resuspended in 10 ml of PBS. Membrane-associated (Pellet) and soluble (Sol.) proteins were separated by centrifugation for 20 min at 12,000 × *g*.

Total protein concentrations were measured by the method of Bradford (Bio-Rad). Proteins were separated by 16% SDS-PAGE, transferred to nitrocellulose membranes, and incubated with the primary antibodies diluted in PBS–5% milk–0.01% Tween 20 (Sigma) overnight. Membranes were washed in PBS three times and then incubated with secondary antibodies for 1 h before washing. Antibody binding was detected with chemiluminescence (ECL kit; GE Healthcare).

FtsZ polymer sedimentation assay. FtsZ polymers (P) were generated in a reaction mixture containing 50 mM HEPES, 50 mM KCl, and 5 mM $MgCl_2$ in addition to 1 mM GTP during 3 min at 30°C and collected by ultracentrifugation (11 min, 80,000 rpm) at 4°C (TL-100 Ultracentrifuge; Beckman). The reactive buffer was then discarded and replaced by a reaction mixture containing 50 mM HEPES, 50 mM KCl, and 5 mM $MgCl_2$ in addition to 1 mM ATP and 0.5 μg/ml of purified ZapE-H_6 when indicated in a final volume of 100 μl. The reaction was stopped after 0, 1, or 3 min, as indicated. FtsZ polymers containing the pellet fraction (P) were separated from the soluble fraction (S) by ultracentrifugation (11 min, 80,000 rpm) at 4°C (TL-100 Ultracentrifuge; Beckman). Samples were resuspended in a Laemli buffer (1× final concentration) and subsequently subjected to SDS-PAGE gel analysis and transferred onto a nitrocellulose membrane. FtsZ and ZapE-H_6 were detected in both fractions by Western blotting using rabbit polyclonal antibodies.

Bioinformatics. Identification of ZapE homologous proteins among other organisms was performed using BlastP. The ZapE sequence comparisons were performed using ClustalW software. Length measurement of bacteria was performed with MicrobeTracker suite software (version 0.937) (15, 17, 31), and the data mining was performed using a MatLab computing system (R2012 version with Image Processing Toolbox and Statistics Toolbox). Statistical analyses were performed using GraphPad Prism 5 software.

Fluorescent protein fusion imaging. In order to localize FtsZ-GFP and ZapE-mCherry and mutated versions of protein fusions in bacteria, the corresponding expression plasmids were transformed in *E. coli* K-12 MG1655 wild-type or Δ*ZapE* strains, as indicated. The localization was performed on either fixed or living bacteria. The fixation of bacteria was performed by adding 4% paraformaldehyde (PFA) followed by a washing in PBS. The observation was performed using a Nikon Eclipse 80i or an

epifluorescence microscope. The live observation of FtsZ-GFP and ZapE-mCherry during the cell division process was performed on an LB agarose (1%) pad using a 200 M Axiovert epifluorescence microscope (Zeiss) equipped with a Lambda LS 300W Xenon lamp and a CoolSnapHQ charge-coupled-device (CCD) camera.

In order to localize FtsZ-mCherry (pAKF133) in K-12 and K12::ΔzapE strains, bacteria were grown in an M9 minimum media at 37°C until an OD_{600} of 0.5 was reached and were further incubated on a minimal medium agar pad with 0.01% arabinose. The cell division process was observed using an inverted microscope (Nikon Ti) equipped with a 100× 1.4 numerical aperture (NA) PL-APO objective lens. Image stacks were acquired using Metamorph software (MDS) and a CCD camera (Photometrics Coolsnap HQ). A similar procedure was applied to observe the effect of ZapE-H_6 overexpression on FtsZ-mCherry localization, through the addition of IPTG (1 mM) within the minimal medium agar pad with 0.01% arabinose (no IPTG was added during the liquid culture growth).

Image reconstruction (see Movie S3 in the supplemental material) was performed using Imaris software (Bitplane).

SUPPLEMENTAL MATERIAL

Supplemental material for this article may be found at http://mbio.asm.org/lookup/suppl/doi:10.1128/mBio.00022-14/-/DCSupplemental.

Movie S1, MOV file, 0.4 MB.
Movie S2, MOV file, 1.9 MB.
Movie S3, MOV file, 5.7 MB.
Figure S1, JPG file, 0.1 MB.
Figure S2, JPG file, 0.1 MB.
Figure S3, JPG file, 0.1 MB.
Figure S4, JPG file, 0.2 MB.
Figure S5, JPG file, 0.1 MB.
Table S1, DOCX file, 0.1 MB.
Text S1, DOCX file, 0.1 MB.

ACKNOWLEDGMENTS

We acknowledge access to the Protein Science Facility, Karolinska Institutet. We gratefully thank Jeff Errington for his initial interest in this project. We thank William Margolin for biochemistry advice. We thank David Weiss for supplying the various Fts protein fusions. We thank Arnaud Echard for scientific discussions and advice. We gratefully acknowledge the synchrotron beamline and excellent user support at the ESRF BioSAXS BM29 beamline. We thank Carmen R. Beuzón López and Spyridoula Charova for offering part of their beam time for the ZapE measurements.

B.S.M. and P.S.J. were supported by EU ERC Homeoepith grant no. 272398 and EU FP7 Tornado grant no. 222720.

REFERENCES

1. **Bi EF, Lutkenhaus J.** 1991. FtsZ ring structure associated with division in Escherichia coli. Nature **354:**161–164. http://dx.doi.org/10.1038/354161a0.
2. **de Boer PA.** 2010. Advances in understanding E. coli cell fission. Curr. Opin. Microbiol. **13:**730–737. http://dx.doi.org/10.1016/j.mib.2010.09.015.
3. **Lutkenhaus J, Pichoff S, Du S.** 2012. Bacterial cytokinesis: from Z ring to divisome. Cytoskeleton (Hoboken) **69:**778–790. http://dx.doi.org/10.1002/cm.21054.
4. **Galli E, Gerdes K.** 2010. Spatial resolution of two bacterial cell division proteins: ZapA recruits ZapB to the inner face of the Z-ring. Mol. Microbiol. **76:**1514–1526. http://dx.doi.org/10.1111/j.1365-2958.2010.07183.x.
5. **Hale CA, Shiomi D, Liu B, Bernhardt TG, Margolin W, Niki H, de Boer PA.** 2011. Identification of Escherichia coli ZapC (YcbW) as a component of the division apparatus that binds and bundles FtsZ polymers. J. Bacteriol. **193:**1393–1404. http://dx.doi.org/10.1128/JB.01245-10.
6. **Durand-Heredia J, Rivkin E, Fan G, Morales J, Janakiraman A.** 2012. Identification of ZapD as a cell division factor that promotes the assembly of FtsZ in Escherichia coli. J. Bacteriol. **194:**3189–3198. http://dx.doi.org/10.1128/JB.00176-12.
7. **Marteyn B, Scorza FB, Sansonetti PJ, Tang C.** 2011. Breathing life into pathogens: the influence of oxygen on bacterial virulence and host responses in the gastrointestinal tract. Cell. Microbiol. **13:**171–176. doi: 10.1111/j.1462-5822.2010.01549.x.
8. **Jones SA, Chowdhury FZ, Fabich AJ, Anderson A, Schreiner DM, House AL, Autieri SM, Leatham MP, Lins JJ, Jorgensen M, Cohen PS, Conway T.** 2007. Respiration of Escherichia coli in the mouse intestine. Infect. Immun. **75:**4891–4899. http://dx.doi.org/10.1128/IAI.00484-07.
9. **West NP, Sansonetti P, Mounier J, Exley RM, Parsot C, Guadagnini S, Prévost MC, Prochnicka-Chalufour A, Delepierre M, Tanguy M, Tang CM.** 2005. Optimization of virulence functions through glucosylation of Shigella LPS. Science **307:**1313–1317. http://dx.doi.org/10.1126/science.1108472.
10. **Marteyn B, West NP, Browning DF, Cole JA, Shaw JG, Palm F, Mounier J, Prévost MC, Sansonetti P, Tang CM.** 2010. Modulation of Shigella virulence in response to available oxygen in vivo. Nature **465:**355–358. http://dx.doi.org/10.1038/nature08970.
11. **Anilkumar G, Srinivasan R, Anand SP, Ajitkumar P.** 2001. Bacterial cell division protein FtsZ is a specific substrate for the AAA family protease FtsH. Microbiology **147**(Pt 3):516–517. http://dx.doi.org/10.1002/jobm.200610236.
12. **Srinivasan R, Ajitkumar P.** 2007. Bacterial cell division protein FtsZ is stable against degradation by AAA family protease FtsH in Escherichia coli cells. J. Basic Microbiol. **47:**251–259. http://dx.doi.org/10.1002/jobm.200610236.
13. **Karimova G, Pidoux J, Ullmann A, Ladant D.** 1998. A bacterial two-hybrid system based on a reconstituted signal transduction pathway. Proc. Natl. Acad. Sci. U. S. A. **95:**5752–5756. http://dx.doi.org/10.1073/pnas.95.10.5752.
14. **Szwedziak P, Wang Q, Freund SM, Löwe J.** 2012. FtsA forms actin-like protofilaments. EMBO J. **31:**2249–2260. http://dx.doi.org/10.1038/emboj.2012.76.
15. **Stouf M, Meile JC, Cornet F.** 2013. FtsK actively segregates sister chromosomes in Escherichia coli. Proc. Natl. Acad. Sci. U. S. A. **110:**11157–11162. http://dx.doi.org/10.1073/pnas.1304080110.
16. **Karimova G, Dautin N, Ladant D.** 2005. Interaction network among Escherichia coli membrane proteins involved in cell division as revealed by bacterial two-hybrid analysis. J. Bacteriol. **187:**2233–2243. http://dx.doi.org/10.1128/JB.187.7.2233-2243.2005.
17. **Weiss DS, Chen JC, Ghigo JM, Boyd D, Beckwith J.** 1999. Localization of FtsI (PBP3) to the septal ring requires its membrane anchor, the Z ring, FtsA, FtsQ, and FtsL. J. Bacteriol. **181:**508–520.
18. **Thanedar S, Margolin W.** 2004. FtsZ exhibits rapid movement and oscillation waves in helix-like patterns in Escherichia coli. Curr. Biol. **14:**1167–1173. http://dx.doi.org/10.1016/j.cub.2004.06.048.
19. **Yu XC, Margolin W.** 1997. Ca2+-mediated GTP-dependent dynamic assembly of bacterial cell division protein FtsZ into asters and polymer networks *in vitro*. EMBO J. **16:**5455–5463. http://dx.doi.org/10.1093/emboj/16.17.5455.
20. **Wu W, Park KT, Holyoak T, Lutkenhaus J.** 2011. Determination of the structure of the MinD-ATP complex reveals the orientation of MinD on the membrane and the relative location of the binding sites for MinE and MinC. Mol. Microbiol. **79:**1515–1528. http://dx.doi.org/10.1111/j.1365-2958.2010.07536.x.
21. **Dong G, Yang Q, Wang Q, Kim YI, Wood TL, Osteryoung KW, van Oudenaarden A, Golden SS.** 2010. Elevated ATPase activity of KaiC applies a circadian checkpoint on cell division in Synechococcus elongatus. Cell **140:**529–539. http://dx.doi.org/10.1016/j.cell.2009.12.042.
22. **Errington J, Daniel RA, Scheffers DJ.** 2003. Cytokinesis in bacteria. Microbiol. Mol. Biol. Rev. **67:**52–65. http://dx.doi.org/10.1128/MMBR.67.1.52-65.2003.
23. **Scheffers D, Driessen AJ.** 2001. The polymerization mechanism of the bacterial cell division protein FtsZ. FEBS Lett. **506:**6–10. http://dx.doi.org/10.1016/S0014-5793(01)02855-1.
24. **Baba T, Ara T, Hasegawa M, Takai Y, Okumura Y, Baba M, Datsenko KA, Tomita M, Wanner BL, Mori H.** 2006. Construction of Escherichia coli K-12 in-frame, single-gene knockout mutants: the Keio collection. Mol. Syst. Biol. **2:**2006.0008. http://dx.doi.org/10.1038/msb4100050.
25. **Miller VL, Beer KB, Loomis WP, Olson JA, Miller SI.** 1992. An unusual pagC::TnphoA mutation leads to an invasion- and virulence-defective phenotype in Salmonellae. Infect. Immun. **60:**3763–3770.
26. **Cherepanov PP, Wackernagel W.** 1995. Gene disruption in Escherichia coli: TcR and KmR cassettes with the option of Flp-catalyzed excision of

the antibiotic-resistance determinant. Gene **158:**9–14. http://dx.doi.org/10.1016/0378-1119(95)00193-A.
27. **Martinez E, Bartolomé B, de la Cruz F.** 1988. pACYC184-derived cloning vectors containing the multiple cloning site and lacZ alpha reporter gene of pUC8/9 and pUC18/19 plasmids. Gene **68:**159–162.
28. **Valdivia RH, Falkow S.** 1996. Bacterial genetics by flow cytometry: rapid isolation of Salmonella typhimurium acid-inducible promoters by differential fluorescence induction. Mol. Microbiol. **22:**367–378. http://dx.doi.org/10.1046/j.1365-2958.1996.00120.x.
29. **Sansonetti PJ, d'Hauteville H, Formal SB, Toucas M.** 1982. Plasmid-mediated invasiveness of "Shigella-like" Escherichia coli. Ann. Microbiol. (Paris) **133:**351–355.
30. **Yu XC, Margolin W.** 1997. Ca2+-mediated GTP-dependent dynamic assembly of bacterial cell division protein FtsZ into asters and polymer networks in vitro. EMBO J. **16:**5455–5463. http://dx.doi.org/10.1093/emboj/16.17.5455.
31. **Sliusarenko O, Heinritz J, Emonet T, Jacobs-Wagner C.** 2011. High-throughput, subpixel precision analysis of bacterial morphogenesis and intracellular spatio-temporal dynamics. Mol. Microbiol. **80:**612–627. http://dx.doi.org/10.1111/j.1365-2958.2011.07579.x.